9604 *Biochemistry* **2010,** *49,* 9604–9612
DOI: 10.1021/bi101168c

BIOCHEMISTRY
including biophysical chemistry & molecular biology
Article

Binding of Reduced Nicotinamide Adenine Dinucleotide Phosphate Destabilizes the Iron−Sulfur Clusters of Human MitoNEET[†]

Tao Zhou, Jinzhong Lin, Yingang Feng, and Jinfeng Wang*

National Laboratory of Biomacromolecules, Institute of Biophysics, Chinese Academy of Sciences, 15 Datun Road, Beijing 100101, China

Received May 10, 2010; Revised Manuscript Received September 26, 2010

ABSTRACT: The outer mitochondrial membrane protein mitoNEET is a cellular target of the antidiabetic drug pioglitazone. Binding of pioglitazone stabilizes the protein against [2Fe-2S] cluster release. Here, we report that reduced nicotinamide adenine dinucleotide phosphate (NADPH) can bind to homodimeric mitoNEET, influencing the stability of the [2Fe-2S] cluster that is bound within a loop region (Y71−H87) in each subunit. Nuclear magnetic resonance (NMR) and isothermal titration calorimetry experiments demonstrated that NADPH binds weakly to mitoNEET(44−108), a soluble domain of mitoNEET containing residues 44−108. Visible−UV absorption measurements revealed the destabilizing effect of NADP binding on the [2Fe-2S] clusters. Disruption of the three-dimensional structure of mitoNEET(44−108) as a result of decomposition of the iron−sulfur clusters was observed by NMR and circular dichroism experiments. Binding of NADPH facilitated release of the iron−sulfur clusters from the protein at pH ≤7.0. Residues K55 and H58 of each subunit of mitoNEET were shown to be involved in NADPH binding. NADPH binding may perturb the interactions of K55 and H58 from one subunit with H87′ and R73′, respectively, from the other subunit, thereby interfering with [2Fe-2S] cluster binding. This may account for the destabilization effect of NADPH binding on the [2Fe-2S] clusters.

MitoNEET was found to be a potential target of the antidiabetic drug pioglitazone, a member of the thiazolidinedione (TZD) family of drugs (*1*). Prior to this discovery, experimental evidence, especially the publication of the structure of a complex between PPARgama and rosiglitazone (*2*), suggested that PPARgama was the main target of TZD drugs. Recent findings have shown that mitoNEET belongs to a new family of iron−sulfur proteins located in the outer mitochondrial membrane. MitoNEET may function in Fe−S cluster shuttling and/or in redox reactions and may play a critical role in proper mitochondrial function (*3*, *4*). The overall structure of the mitoNEET soluble domain appears to be a homodimer with one [2Fe-2S] cluster in each monomer subunit (*5*−*7*). Each [2Fe-2S] cluster is coordinated by three cysteines and one histidine within a stretch of 17 consecutive residues (residues Y71−H87) from loop L3 (residues Y71−G85) and the N-terminus of helix α1 (residues A86−G95). The [2Fe-2S] cluster was found to be surprisingly pH-labile at pH ≤8.0 and is linked to the protonation of H87 upon acidification. Loss of the ligand H87 via protonation can trigger the release of the [2Fe-2S] cluster, and the stability of the [2Fe-2S] cluster is increased in an H87C mutant of mitoNEET (*3*), which is attributed to a specific change in the ligation of the [2Fe-2S] cluster and not to a more global conformational change (*8*). Resonance Raman studies suggested that the Fe−N(H87) interaction is modulated within the physiological pH range, and that this modulation may be critical to the function of mitoNEET (*9*). The pH-dependent redox potential of mitoNEET was determined to be 35 mV at pH 7.5 and was ∼40 mV lower in the presence of phosphate ions. Phosphate at physiological concentrations can stabilize the cluster from release over a pH range of 5.0−7.5 (*10*, *11*). Pioglitazone has been shown to stabilize the uniquely coordinated [2Fe-2S] clusters of mitoNEET (*5*).

Here, we report new findings that NADP(H),[1] a coenzyme involved in metabolic processes, can bind weakly to mitoNEET, destabilizing the [2Fe-2S] clusters of the protein. A soluble domain of human mitoNEET containing residues 44−108, named mitoNEET(44−108), was used in this study. Heteronuclear NMR experiments and ITC, visible−UV absorption, and CD measurements were performed to investigate the binding of NADP(H) and its effect on the stability of the [2Fe-2S] clusters in mitoNEET. Residues of mitoNEET(44−108) involved in the binding of NADP(H) were determined by NMR titration experiments. Results revealed that binding of NADP(H) facilitated release of the [2Fe-2S] cluster from mitoNEET(44−108). Residues K55 and H58 are proposed to be responsible for the destabilization of the iron−sulfur clusters of mitoNEET by binding of NADP(H).

MATERIALS AND METHODS

Protein Preparation. MitoNEET is located in the mitochondria by an N-terminal targeting sequence that acts as a membrane tether, resulting in the majority of the protein being exposed to the cytoplasm (*4*). The crystal homodimeric structure of human mitoNEET was determined for the truncated protein (residues

[†]This research was supported by the National Natural Science Foundation of China (NNSFC 30770434).

*To whom correspondence should be addressed. E-mail: jfw@sun5.ibp.ac.cn. Phone: +86-10-64888490. Fax: +86-10-64872026.

[1]Abbreviations: NADP, nicotinamide adenine dinucleotide phosphate; NADPH, reduced nicotinamide adenine dinucleotide phosphate; NADH, reduced nicotinamide adenine dinucleotide; IPTG, isopropyl β-D-thiogalactopyranoside; ITC, isothermal titration calorimetry; CD, circular dichroism; DSS, 2,2-dimethyl-2-silapentane 5-sulfonate.

 Published on Web 10/11/2010 © 2010 American Chemical Society

32−108 of full-length mitoNEET). Residues 32−42 of one monomer and 32−37 of the other monomer in the structure are known to be very flexible because no electronic density is observed for these residues (*6*). Because the amino acid in position 44 is methionine, a soluble domain of human mitoNEET containing residues 44−108, mitoNEET(44−108), was amplified by polymerase chain reaction (PCR) and cloned into the pET-22b vector (Novagen) to obtain a better two-dimensional (2D) $^{1}H-^{15}N$ HSQC spectrum of mitoNEET. Mutant variants [R76Q/K78Q/K89Q]mitoNEET(44−108) and [K55Q/H58S]-mitoNEET(44−108) were produced via the introduction of R76Q, K78Q, and K89Q mutations and K55Q and H58S mutations of mitoNEET(44−108), respectively, into the pET22b-mitoNEET(44−108) plasmid by overlap extension using PCR (*12*).

The recombinant pET22b-mitoNEET(44−108) plasmids were transformed into *Escherichia coli* expression strain BL21(DE3) cells, and cells were cultured at 37 °C. When the optical density at 600 nm (OD_{600}) reached 0.8, protein expression was induced by addition of 0.4 mM IPTG. Cells were harvested by centrifugation after 3 h and lysed by sonication in buffer A [20 mM Tris-HCl (pH 7.9), 5 mM imidazole, and 500 mM NaCl]. The lysate was first applied to a Ni-NTA column pre-equilibrated with buffer A, which was then washed with buffer A containing 30 mM imidazole. The protein was then eluted with buffer A containing 500 mM imidazole and purified by gel filtration chromatography using a Superdex 75 column (Amersham Biosciences) with 150 mM ammonium bicarbonate. The purified protein was lyophilized and stored at −20 °C. Recombinant mitoNEET(44−108) contains eight additional C-terminal residues derived from the His tag (LEHHHHHH).

Uniformly ^{15}N-labeled mitoNEET(44−108) and ^{15}N- and ^{13}C-labeled mitoNEET(44−108) were obtained by bacterial growth in M9 minimal medium containing $^{15}NH_4Cl$ and [^{13}C]glucose as the sole nitrogen and carbon sources, respectively. Protein purity was confirmed by sodium dodecyl sulfate−polyacrylamide gel electrophoresis.

The apparent molecular mass [$M_{r(app)}$] of mitoNEET(44−108) was estimated to verify that mitoNEET(44−108) was homodimeric. Analytical ultracentrifugation experiments were performed with a Beckman XL-I centrifuge at 60000 rpm using an AN60Ti rotor and two channel cells. Sedimentation velocities were measured at a protein concentration of 80 μM. The protein was dissolved in three different buffers at 20 °C: 50 mM sodium phosphate and 50 mM KCl (pH 7.0), 50 mM sodium phosphate and 50 mM KCl (pH 7.5), and 20 mM Tris-HCl and 150 mM NaCl (pH 8.0). The estimated $M_{r(app)}$ of mitoNEET(44−108) at different pH values was 17.4 ± 0.7 kDa at pH 7.0, 17.1 ± 0.7 kDa at pH 7.5, and 17.4 ± 0.8 kDa at pH 8.0. Therefore, because monomeric mitoNEET(44−108) has a calculated molecular mass of 8.6 kDa, the purified mitoNEET(44−108) indeed forms homodimers in aqueous solution. The protein concentrations of all samples used in this study are given in terms of monomer equivalents.

NMR Spectroscopy. All NMR experiments were conducted on a Bruker DMX600 spectrometer equipped with a triple-resonance cryoprobe. The three-dimensional (3D) $^{1}H-^{15}N-^{13}C$ HNCACB, CBCA(CO)NH, HNCA, HN(CA)CO, and HNCO experiments for backbone resonance assignments were conducted at 303 K. The sample used for these NMR experiments was 1.0 mM doubly ^{15}N- and ^{13}C-labeled mitoNEET(44−108) dissolved in a 90% H_2O/10% D_2O mixture containing 50 mM sodium phosphate (pH 7.5), 50 mM KCl, and 0.02% NaN_3, unless otherwise indicated. For investigation of protein stability over time, 2D $^{1}H-^{15}N$ HSQC experiments were performed at 303 K with 0.2 mM ^{15}N-labeled mitoNEET(44−108) dissolved in a 90% H_2O/10% D_2O mixture containing 100 mM citric acid (pH 6.0), 50 mM KCl, and 0.02% NaN_3. Stability measurements were taken over a period of 20 h; spectra were recorded each hour for the first 15 h and then 20 h after the start of the measurements.

All the collected NMR data were processed and analyzed using FELIX98 (Accelrys Inc.). ^{1}H chemical shifts were calibrated relative to internal 0.25 mM DSS. ^{15}N and ^{13}C chemical shifts were referenced indirectly (*13*).

NMR Titration Experiments. Titration of mitoNEET-(44−108) with NADPH and NADP (Biomol) was monitored by 2D $^{1}H-^{15}N$ HSQC spectra of titrated mitoNEET(44−108) recorded at 303 K. For the titration experiments, the mitoNEET-(44−108) sample solution (4.0 mL), prepared by dissolving 0.2 mM ^{15}N-labeled mitoNEET(44−108) in NMR buffer [50 mM sodium phosphate (pH 7.0), 50 mM KCl, 0.02% NaN_3, and a 90% H_2O/10% D_2O mixture], was divided into eight aliquots. Concentrated solutions of NADPH and NADP were freshly prepared in NMR buffer. Aliquots of these concentrated solutions were added to each mitoNEET(44−108) sample solution to achieve the desired concentrations of 0.2, 0.4, 0.8, 1.6, 3.2, 6.4, and 12.8 mM. Chemical shift titration data were analyzed, and weighted chemical shift changes were calculated according to the equation $\Delta\delta = [(5\Delta\delta^{1}H)^2 + (\Delta\delta^{15}N)^2]^{1/2}$ (*14*). For comparison, titration of mitoNEET(44−108) with NADPH and NADH and with PO_4^{3-} was conducted in 25 mM HEPES buffer containing 50 mM KCl (pH 8.0).

The pH dependence of cluster stability was monitored using the 2D $^{1}H-^{15}N$ HSQC spectra of mitoNEET(44−108) recorded at 303 K. Titration measurements were taken over a pH range from pH 8.0 to 5.0. Six aliquots of mitoNEET(44−108) were dissolved in a 90% H_2O/10% D_2O mixture containing 25 mM HEPES and 50 mM KCl at pH 8.0, 7.5, 7.0, 6.5, 6.0, and 5.0. The protein concentration of each sample was 0.2 mM. Each sample was incubated for a fixed time of 15 min before being subjected to 2D $^{1}H-^{15}N$ HSQC spectroscopy for ∼45 min.

Isothermal Titration Calorimetry. Isothermal titration calorimetry (ITC) was used for detecting the interactions of mitoNEET(44−108) and its mutant variants [R76Q/K78Q/K89Q] mitoNEET(44−108) and [K55Q/H58S]mitoNEET(44−108) with NADPH and NADP. For comparison, the interaction of mitoNEET(44−108) with NADH was also examined by ITC. The ITC measurements were taken at 25 °C on an iTC_{200} microcalorimeter (MicroCal Inc.). The sample cell was loaded with 200 μL of sample solution prepared by dissolving 2.0 mM mitoNEET-(44−108) in a buffer [50 mM sodium phosphate (pH 7.0) and 50 mM KCl], and the reference cell contained only doubly distilled water; 50 mM NADPH and NADP or NADH, dissolved in the same buffer as the protein, were inserted into the sample cell using a syringe, and the mixture was stirred at 1000 rpm. Thirty-eight 1 μL drops were successively injected at 150 s intervals (to allow the trace to return to baseline). Control experiments were performed via injection of the ligand into buffer alone in the sample cell, and the heat of dilution was subtracted from the protein−ligand titration data. All solutions were degassed for 10 min to remove bubbles under vacuum prior to being used.

Microcal Origin was used to analyze the titration data. The estimated from the fitted titration curve. The binding Gibbs free energy (ΔG) was determined using the standard relationship $\Delta G = -RT \ln(1/K_d)$, where R is the gas constant and T is the

absolute temperature. The resultant association entropy (ΔS) was calculated using the standard thermodynamic relationship $T\Delta S = \Delta H - \Delta G$.

Visible−UV Absorption Measurement. To monitor the stability of [2Fe-2S] clusters in the mitoNEET(44−108) molecule, we measured the visible−UV absorbance at 460 nm (A_{460}) at 25 °C. Release of [2Fe-2S] clusters from mitoNEET(44−108) was detected by a decrease in A_{460} over time (*3*). The measurements were taken on a U-2010 Hitachi spectrophotometer with 1 cm cells. Samples used for stability measurements contained 0.2 mM mitoNEET(44−108) in 100 mM sodium citrate buffer (pH 6.0) or in 100 mM sodium citrate mixed with 50 mM sodium phosphate (pH 7.0) containing 50 mM KCl in the presence or absence of 10 mM NADP and PO_4^{3-}, and 0.2 mM [K55Q/H58S]mitoNEET-(44−108) in 100 mM sodium citrate mixed with 50 mM sodium phosphate (pH 7.0) containing 50 mM KCl. Spectra were recorded using three replicates for each sample. The pH was the same at the beginning and end of each measurement. Absorption spectra were recorded at successive time intervals, as indicated.

Circular Dichroism (*CD*). Far-UV CD (190−260 nm) and near-UV CD (340−250 nm) spectra were used to detect structural changes due to the release of the [2Fe-2S] cluster from mitoNEET-(44−108). Samples used for CD measurements contained 0.1 mM protein in 50 mM sodium phosphate buffer containing 50 mM KCl. Experiments were performed on an Applied Photophysics PiStar CD spectrometer at 25 °C using samples in the pH range of 6.0−8.0 (at pH 0.5 intervals). Cuvette path lengths of 0.1 and 10.0 mm were employed for far-UV and near-UV CD measurements, respectively. Five spectral scans were run and averaged for each measurement.

RESULTS

Interaction of NADPH and NADP with MitoNEET-(44−108). Interactions of NADPH and NADP with mito-NEET(44−108) were detected by NMR titration experiments. The cross-peaks in the 2D $^1H-^{15}N$ HSQC spectrum of mito-NEET(44−108) shifted upon interaction with NADPH and NADP. Figure 1A shows the assignment of resonances for back-bone amide groups of mitoNEET(44−108). Because of the influence of paramagnetic Fe^{3+} in the [2Fe-2S] cluster, resonance signals for the [2Fe-2S] cluster binding of residues in the V70−N91 segment, including 17 consecutive residues (Y71−H87), were missing in the spectrum. In addition, the amino acids at sequence positions 54 and 100 are prolines, and cross-peaks for residues G99 and L101 around P100 could not be assigned.

In the titration of mitoNEET(44−108) with NADPH and NADP, the 2D $^1H-^{15}N$ HSQC spectra of mitoNEET(44−108) recorded in sodium phosphate buffer (pH 7.0) showed shifting of resonance signals for several residues as the concentration of NADPH (Figure 1B) or NADP (data not shown) increased. Relatively significant changes in chemical shifts of ^1H_N and ^{15}N resonances were observed for residues K55, V57, H58, K68, A69, I102, I103, K105, and E107 in the titration with NADPH (Figure 1B,C). Actually, only some of these residues interact directly with NADPH, but they may influence the chemical shifts of the resonances of the other residues. The dissociation constant K_d of NADPH with mitoNEET(44−108) was obtained by fitting the chemical shift changes of amide group resonances for residues K55, H58, K68, and I102 (Figure 1D), assuming a single binding mode (see below). Maximal chemical shift changes (Table S1 of the Supporting Information) indicated that K55 and H58 were the two residues most sensitive to NADPH binding. Averaging the K_d values obtained for these four residues gave a value of 1.99 ± 0.15 mM, which is similar to that obtained from ITC measurements (see below).

In addition, titration of NADP with mitoNEET(44−108) was performed using one-dimensional (1D) ^1H NMR. The 1D ^1H NMR spectra of NADP showed changes in the chemical shift of the adenine A8 resonance and progressive line broadening of the ribose A1′ resonance in the adenosine moiety of NADP as the concentration of mitoNEET(44−108) increased (Figure S1 of the Supporting Information). This strongly suggested the direct binding of the adenosine moiety of NADP to mitoNEET(44−108). Titration experiments with NADPH gave the same result (data not shown).

However, when mitoNEET(44−108) was titrated with NADH and phosphate ion PO_4^{3-} in 25 mM HEPES buffer (a phosphate ion-free buffer), the 2D $^1H-^{15}N$ HSQC spectra of mitoNEET-(44−108) did not show shifting of resonance signals as the concentrations of NADH and PO_4^{3-} increased (Figure S2 of the Supporting Information). It seems the phosphate ion does not show distinct interactions with the surface residues of the protein, and the interaction of NADH with mitoNEET(44−108) was also unable to influence the chemical shifts of the resonances. Therefore, only NADP(H) but not NADH can interact with mitoNEET-(44−108), influencing the chemical shifts of the resonances for the residues mentioned above. This implies that mitoNEET binds with NADP(H) but not NADH.

Calorimetric Analysis of the Binding of NADPH with MitoNEET(44−108). Thermodynamic information obtained from ITC can be used to characterize the binding of NADPH and NADP to mitoNEET(44−108). Figure 2 shows a representative ITC profile obtained for the interaction of NADPH with mitoNEET(44−108) at pH 7.0, which is characterized by a 1:1 stoichiometry. Using a model for one binding site, fitting ITC data gave a dissociation constant (K_d) of 2.12 ± 0.14 mM, indicating that the binding of NADPH with mitoNEET is weak. Analysis of thermodynamic parameters at 25 °C revealed that the weak binding of NADPH to mitoNEET(44−108) was associated with a favorable binding enthalpy ($\Delta H = -6.06 \pm 0.17$ kcal/mol) and an unfavorable binding entropy change ($\Delta S = -8.08$ cal mol^{-1} K^{-1}) (Table S2 of the Supporting Information). It is likely that electrostatic interactions between the surface-charged amino acids (for example, K55, H58, and K68) of the protein and the negative phosphate ion PO_4^{3-} in NADPH make a greater contribution to the binding of NADPH to mitoNEET(44−108). Thus, the favorable binding ΔH may be due to the electrostatics of the surface basic amino acids of the protein and the PO_4^{3-} in NADPH. On the other hand, the unfavorable ΔS for the binding interaction is probably due to the increased order of the NADPH molecule on binding to the protein. A lower binding affinity was observed for the interaction of NADP with mitoNEET(44−108), having a K_d value of 6.49 ± 0.17 mM. However, ITC measurements indicated that NADH was essentially unable to bind with mitoNEET(44−108) (Figure S3 of the Supporting Information). This is consistent with results from NMR titration experiments.

As indicated above, the large changes in the chemical shifts shown by residues K55, H58, K68, A69, I102, I103, and E107 of the protein were due to the binding of NADPH (Figure 1C). However, resonance signals for residues in the cluster binding loop were missing in the NMR spectrum. Inspection of the 3D structure of mitoNEET revealed that most residues in the loop

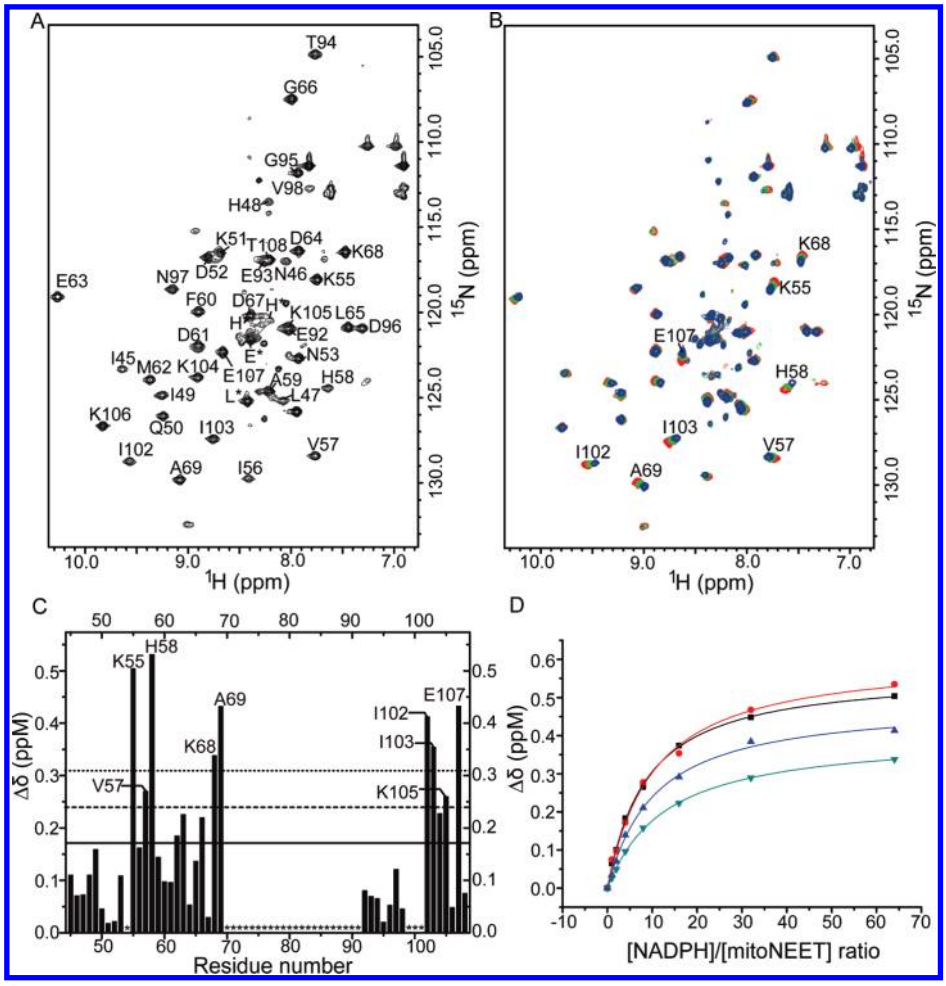

FIGURE 1: Titration of NADPH by monitoring the chemical shift changes of resonance signals in the 2D $^{1}H-^{15}N$ HSQC spectra of mitoNEET(44−108) in sodium phosphate buffer (pH 7.0). (A) Residue-specific assignments for backbone amide groups of mitoNEET(44−108). Assignments are labeled with one-letter amino acid codes and the residue number. Labels (L*, E*, and H*) indicate additional C-terminal residues derived from the His tag. (B) Spectrum of free mitoNEET(44−108) (red) overlaid with the spectra recorded for mitoNEET(44−108) with 1.6 mM NADPH (green) or 12.8 mM NADPH (blue). (C) Weighted chemical shift differences (Δδ) between resonances for mitoNEET(44−108) in the presence of 12.8 mM NADPH and those in the absence of NADPH. Asterisks denote unassigned residues. Solid, dashed, and dotted horizontal lines correspond to the average chemical shift change and 0.5 and 1.0 standard deviation above the average chemical shift change, respectively. (D) Chemical shift changes for K55 (■), H58 (●), K68 (▼), and I102 (▲) as a function of NADPH concentration in the titration experiments. The solid curves are the curve fitting results from the 1:1 binding mode.

are buried inside the protein, and the basic residues, R76, K78, and K79, in the loop and K89 in the N-terminus of the helix are solvent-exposed. R76 and K78 form a cluster with K89. To examine whether these residues can interact with NADPH, thus influencing the stability of the clusters, an R76Q/K78Q/K89Q mutant protein was constructed and subjected to ITC measurements. In addition, because K55 and H58 are the two residues most sensitive to NADPH binding, a K55Q/H58S mutant mitoNEET(44−108) was also constructed and subjected to ITC measurements to acquire further experimental support for interactions of NADPH with residues K55 and H58. Comparison of 1D ^{1}H NMR spectra of these mutant proteins with that of native mitoNEET(44−108) indicates that they fold normally (Figure S4 of the Supporting Information). ITC results demonstrated that binding of NADPH with [R76Q/K78Q/K89Q]mitoNEET(44−108) (Table S2 of the Supporting Information) is similar to that with native mitoNEET(44−108), and that [K55Q/H58S]mitoNEET(44−108) hardly interacts with NADPH (Figure S5 of the Supporting Information). This indicates that K55 and H58 are the two residues crucial for NADPH binding. However, residues R76, K78, and K89 did not play a major role in the binding of NADPH with mitoNEET(44−108), suggesting that NADPH cannot bind directly to the cluster binding loop.

Binding of NADP Facilitates the Release of the Cluster from MitoNEET(44−108). As [2Fe-2S] clusters are gradually released from mitoNEET(44−108) at pH 6.0, the sample solution becomes a mixture of proteins in the unfolded and native folded states (see below). In 2D $^{1}H-^{15}N$ HSQC spectra recorded at pH 6.0, the signal intensity of cross-peaks for mitoNEET(44−108) in the native folded state decreased with time (Figure S6 of the Supporting Information). Release of the [2Fe-2S] clusters over time at pH 6.0 can also be characterized by absorbance at 460 nm (A_{460}) in the UV−visible absorption spectra of mitoNEET(44−108). Decomposition of [2Fe-2S] clusters upon interaction with NADP was demonstrated by the A_{460} for mitoNEET(44−108) in 100 mM citric acid buffer (pH 6.0) and in 100 mM sodium citrate mixed with 50 mM sodium phosphate (pH 7.0) containing 50 mM KCl.

Figure 3A shows UV−visible absorption data for mitoNEET(44−108) obtained using samples prepared in citric acid buffer (pH 6.0). Significant change in A_{460} readings over time was observed for mitoNEET(44−108) in the presence of 10 mM

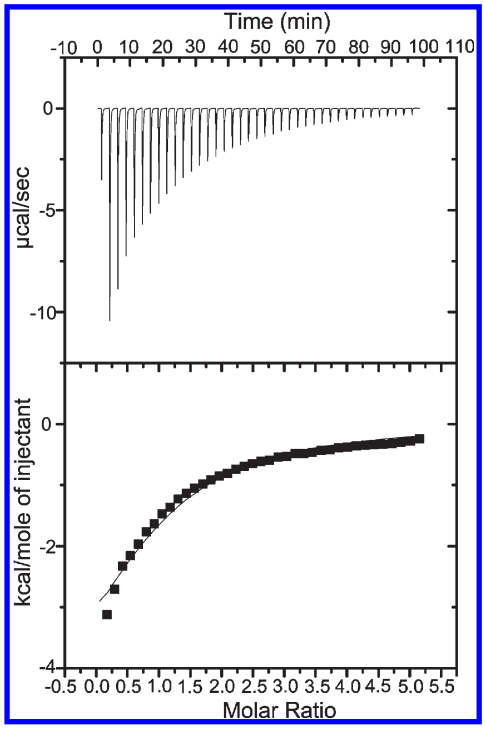

FIGURE 2: Isothermal titration calorimetry profiles for the binding of NADPH to mitoNEET(44−108) at pH 7.0 and 25 °C. The top panel displays the raw data for sequential 1.0 μL injections of 50 mM NADPH into a 1.0 mM mitoNEET(44−108) solution. The first injection consisted of 0.4 μL of NADPH. The bottom panel presents the plot of the heat evolved (kilocalories) per mole of NADPH added, corrected for the heat of NADPH dilution, against the molar ratio of NADPH to mitoNEET(44−108). The data (■) were fitted to a single-site binding model, and the solid line represents the best fit.

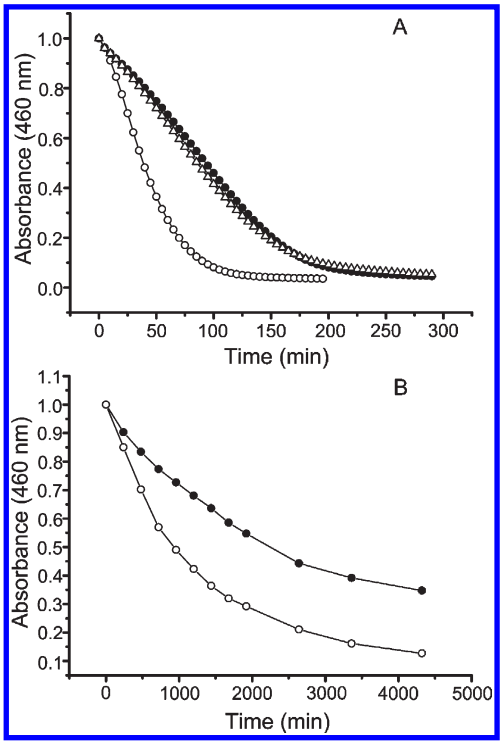

FIGURE 3: UV−visible absorption spectra of mitoNEET(44−108) in citric acid buffer at pH 6.0 (A) and in mixed sodium citrate and sodium phosphate buffers at pH 7.0 (B). Release of [2Fe-2S] clusters was assessed by the absorbance of mitoNEET(44−108) at 460 nm over time in buffer only (●), in the presence of 10 mM NADP (○), and in the presence of 10 mM PO_4^{3-} (△).

NADP compared to mitoNEET(44−108) in the free state and in the presence of 10 mM PO_4^{3-}. The half-life of the [2Fe-2S] clusters ($\tau_{1/2}$) was 38 min for mitoNEET(44−108) with NADP but 92 min for free mitoNEET(44−108). Changes in A_{460} readings over time obtained for the protein in the presence of phosphate ion were very similar to those for free mitoNEET(44−108). Therefore, destabilization of the iron−sulfur clusters in the mitoNEET molecule was enhanced by its interaction with NADP but not the phosphate ion PO_4^{3-} at pH <7.0. At pH 7.0, a relatively fast decay of [2Fe-2S] cluster absorbance was also observed for mitoNEET(44−108) upon interaction with NADP (Figure 3B). Clearly, binding of NADP facilitated release of [2Fe-2S] clusters from mitoNEET-(44−108).

Cluster Release Induces Structural Changes in MitoNEET(44−108). To investigate the influence of the release of [2Fe-2S] clusters on protein structure, pH titrations were performed for mitoNEET(44−108) in HEPES buffer (Figure 4) and in sodium phosphate buffer (data not shown) over a pH range of 5.0−8.0. Figure 4 shows 2D $^1H-^{15}N$ HSQC spectra of mitoNEET(44−108) recorded at pH 8.0, 7.0, 6.0, and 5.0. Compared to the spectra recorded at pH 8.0 (Figure 4A) and pH 7.5 (not shown), that recorded at pH 7.0 (Figure 4B) has a few very weak peaks in the 7.8−8.6 ppm spectral region of ^1H_N resonances. At pH 6.0 (Figure 4C), new peaks appeared in this spectral region in addition to the normal highly dispersed peaks with lower intensity. This may be because the residues surrounding the [2Fe-2S] cluster, including the 17 consecutive residues, Y71−H87, were liberated from the influence of paramagnetic Fe^{3+} due to the degradation of the paramagnetic [2Fe-2S] cluster; however, the protein may still retain some minor conformation.

Results clearly indicate that the [2Fe-2S] clusters were nearly stable at pH 7.0. As the pH was progressively lowered from 6.0 to 5.0, more cross-peaks appeared in this narrow spectral region, and the intensity of the dispersed cross-peaks decreased significantly. This indicates that, at pH <6.0, the decomposition of [2Fe-2S] clusters destroyed the 3D structure of the protein, inducing more complete unfolding of mitoNEET(44−108). At pH 5.0, most of the [2Fe-2S] clusters were released from the protein (the protein sample became a colorless solution after 6 h), and mitoNEET(44−108) was largely unfolded.

According to the X-ray structure of mitoNEET, each monomer subunit of the homodimer comprises one α-helix, one three-stranded β-sheet, and four loops. The N-terminus of the α-helix is involved in [2Fe-2S] cluster binding, and the α-helix is likely to be stabilized by binding of the cluster (*3*, *4*). In agreement with these reports, the far-UV CD spectra of mitoNEET(44−108) at pH 7.5 and 8.0 showed characteristics of a structured α/β protein (Figure 5A). When the pH of the samples was lowered from 8.0 to 6.0, the intensity of the helical bands at 220 nm decreased. At pH 6.0, the ellipticity at 220 nm decreased markedly within 1 h, suggesting that moderate changes occurred in the secondary structures of mitoNEET(44−108). Moreover, random coils were observed in the far-UV CD spectrum of mitoNEET(44−108) after 11 h. These observations indicate that the secondary structure of mitoNEET(44−108) was moderately disrupted at pH 6.0 after 1 h and more or less disappeared after 11 h because of the decomposition of the [2Fe-2S] clusters of the protein.

Near-UV CD spectra can depict conformational changes in the environment of the [2Fe-2S] cluster in mitoNEET(44−108) because residue W75, the only tryptophan amino acid in the protein, is located in the 17-residue cluster binding loop. Figure 5B shows a unique feature of mitoNEET(44−108) at

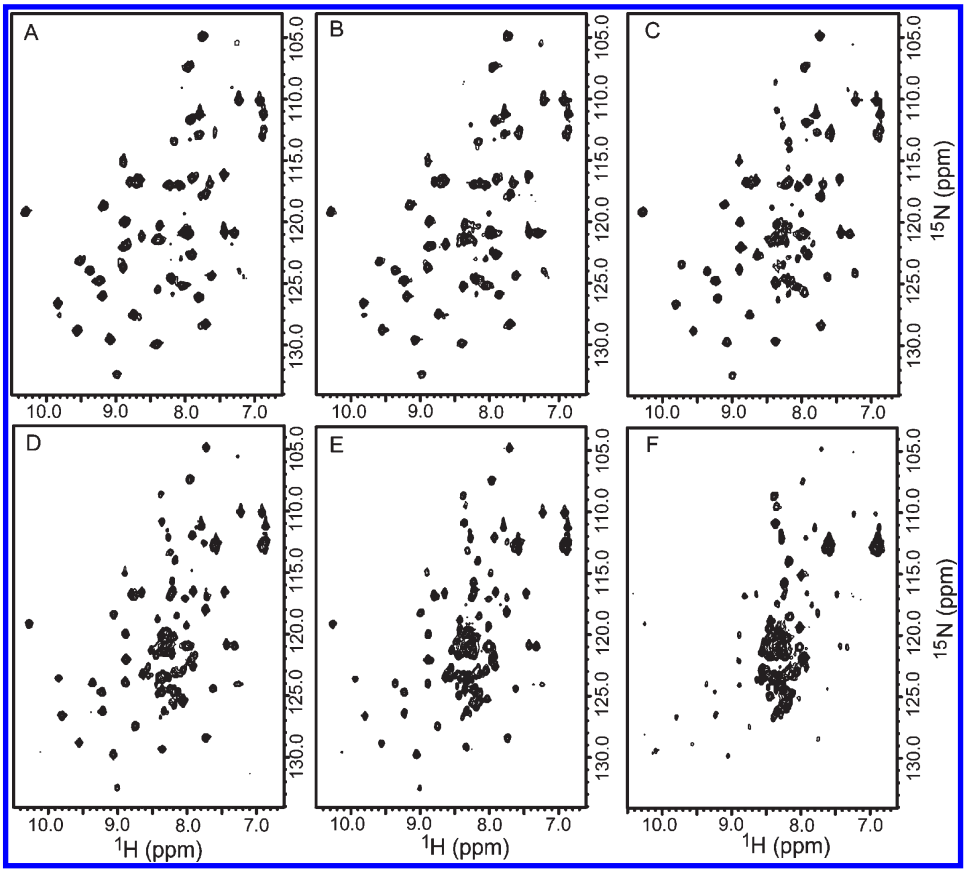

FIGURE 4: 2D ^{1}H−^{15}N HSQC spectra of mitoNEET(44−108) in 25 mM HEPES buffer recorded at pH 8.0 (A), 7.0 (B), 6.0 (C), or 5.0 (D) 1 h after the beginning of the sample preparation, and at pH 5.0 after 2 (E) and 5 h (F).

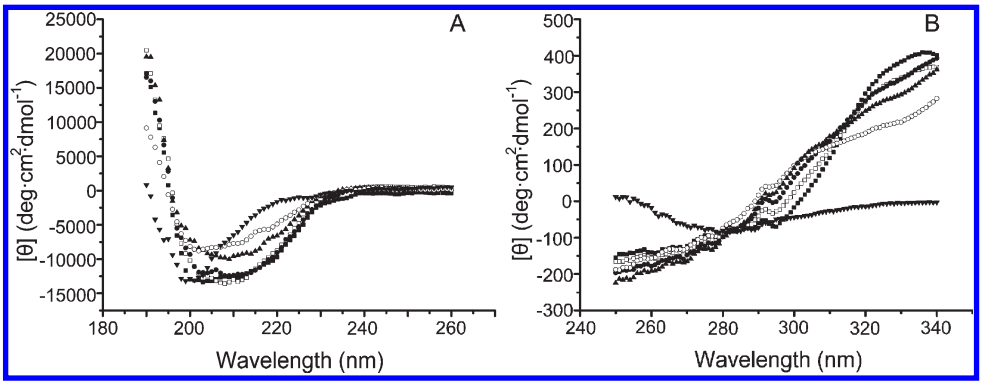

FIGURE 5: CD spectra of mitoNEET(44−108) at different pH values recorded for different lengths of time. Far-UV CD (190−260 nm) (A) and near-UV CD (340−250 nm) (B) spectra recorded within 1 h at pH 8.0 (■), 7.5 (□), 7.0 (●), 6.5 (▲), and 6.0 (○), and after 11 h at pH 6.0 (▼).

pH 8.0 in that it has a positive band near 336 nm and a small negative peak near 294 nm. A strong diminution of the magnitude of the near-UV CD signal was observed for the sample at pH 6.0 after 11 h, indicating intense changes in the environment around the [2Fe-2S] cluster. Therefore, destabilization of the iron−sulfur clusters can induce a global loss of tertiary structure in mitoNEET(44−108).

DISCUSSION

Structural Factors Cause [2Fe-2S] Cluster Destabilization on Binding of NADP(H). The experimental results presented here reveal that binding of NADP facilitates release of [2Fe-2S] clusters from mitoNEET(44−108) (Figure 3). In addition, residues K55, H58, K68, A69, I102, I103, and E107 of the protein were shown to be involved in binding with NADP(H), and the solvent-exposed basic residues surrounding the [2Fe-2S] cluster did not interact significantly with NADPH (Table S2 of the Supporting Information). Phosphate ion in the sample solution did not show distinct interactions with mitoNEET-(44−108) (Figure 3A and Figure S2 of the Supporting Information). These experimental facts strongly suggest that the destabilizing effect of NADP(H) binding on the coordinated clusters of mitoNEET(44−108) must correlate with some of the residues of the protein mentioned above. Of these residues, shifting of the E107 resonance was due to the His tag at the C-terminus of the protein. Removing the His tag also eliminated the chemical shift changes of E107 (data not shown). Residues A69 and I103 are involved in the formation of an intersubunit

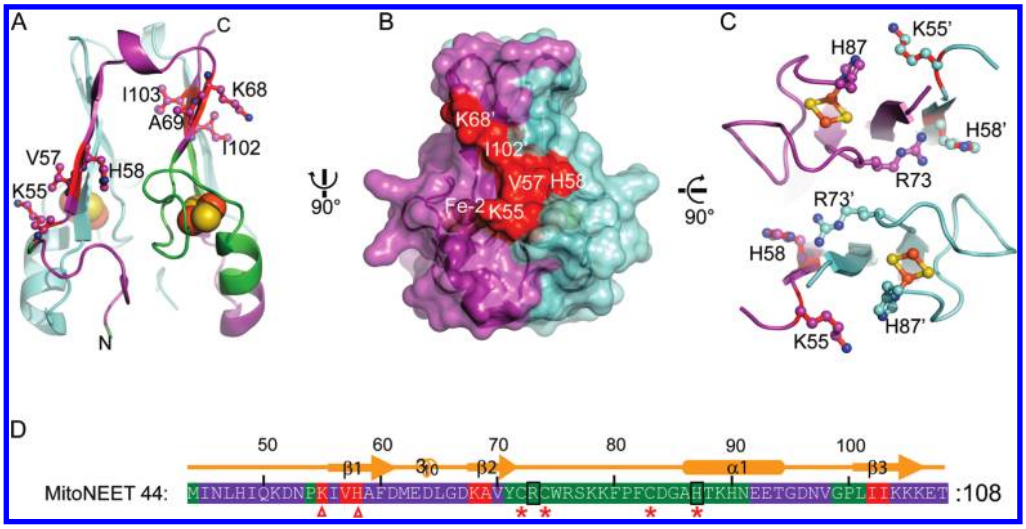

FIGURE 6: NADPH-binding sites on mitoNEET. (A) Ribbon diagram of the dimeric structure of human mitoNEET(44−108). One subunit is colored purple. The backbone tracing of the residues unassigned in the 2D $^{1}H-^{15}N$ HSQC spectrum is colored green. Residues involved in binding with NADPH are shown as balls and sticks and labeled. (B) Surface representation of the dimeric mitoNEET. Residues K55, V57, and H58 from one subunit and residues K68′ and I102′ from the other subunit form a NADPH-binding surface (colored red) at the opening of the [2Fe-2S] cluster. (C) View of the region including residues K55 and H58 from one subunit (purple) and residues R73′ and H87′ from the other subunit (cyan). (D) Sequence of human mitoNEET(44−108). Residues unassigned in the NMR study are highlighted in green, and residues involved in binding with NADPH are highlighted in red. Secondary structural regions are indicated above the sequence. Cluster-coordinating residues are denoted with asterisks. K55 and H58, the two residues most sensitive to NADPH binding, are denoted with red triangles. The two boxed residues are R73 and H87, which are close to residues H58 and K55, respectively, in the dimeric mitoNEET structure.

hydrophobic core in the β-sandwich region (Figure 6A) (*6*). Thus, we conclude that residues K55, H58, K68, and I102 of mitoNEET(44−108) are involved in the direct interaction with NADP(H). By inspection of the mitoNEET structure, residues K55, H58, and V57 from one subunit, together with residues K68′ and I102′ from the other subunit, form a surface on the mitoNEET(44−108) molecule for NADP(H) binding (Figure 6B). Moreover, K55 and H58 are the two major residues responsible for the binding of NADP(H), as verified by ITC measurements of K55Q/H58S mutant mitoNEET (Figure S5 of the Supporting Information). The conserved residues K55, V57, and I102 in mitoNEET homologues are near the opening of the iron−sulfur cluster on the surface of the mitoNEET molecule (*6*).

In the mitoNEET(44−108) structure, residues K55 and H58 from one monomer subunit are close to residues H87′ and R73′, respectively, from the other monomer subunit (Figure 6C). R73 is located between C72 and C74, which, together with H87, are iron ligands of the cluster (Figure 6D). The distances between R73′ NH1 and H58 ND and between R73′ NH2 and H58 ND are 3.07 and 3.08 Å, respectively (*6*). As reported, an unusual intersubunit hydrogen bond within the interior of the protein dimer may be formed between H58 and R73′, enhancing the interaction between the two subunits and the stability of the dimer interface (*5*). Perturbation of this interaction may disrupt the coordination sphere of Fe-1 (coordinated by C72 and C74) in the cluster, influencing cluster binding. With respect to Fe-2 in the cluster, the single histidine ligation (Fe-2 coordinated by H87 and C83) acts on the stability of the cluster. Protonation of H87 could destabilize the helix, facilitating cluster release and/or transfer (*5*). K55 is adjacent to the imidazole ring of H87′, and the K55 NZ−H87′ NE distance is 4.44 Å (*6*). The proximity of the basic residue K55 to H87′ may have some effect on the protonation state of the imidazole ring of histidine. Apparently, the K55Q/H58S mutation of mitoNEET(44−108) may perturb the hydrogen bond between H58 and R73′ and the protonation state of H87. This is evidenced by the relatively fast decay of the [2Fe-2S] cluster absorbance of [K55Q/H58S]mitoNEET(44−108), compared to the A_{460} of native mitoNEET(44−108), due to significant perturbation of the interactions between residues H58−R73′ and K55−H87′ (Figure S7 of the Supporting Information). Binding of NADP(H) to mitoNEET(44−108) presumably influences the side chain conformation of K55 and H58, perturbing the interactions between H58 and R73′ and between K55 and H87′ and thereby interfering with cluster binding. This should account for the destabilization of [2Fe-2S] clusters on binding of NADP(H).

Possible Biological Importance of NADP(H) Binding. Preliminary functional studies have shown that mitoNEET plays an important role in metabolism. Iron−sulfur clusters are known to be essential partners in metabolic processes. That mitoNEET is linked with diabetes, a metabolic disorder, emphasizes the importance of elucidating its exact function. In this study, we found that mitoNEET interacts mainly with NADP(H), not NADH, and that the binding of NADP(H) with mitoNEET destabilizes the [2Fe-2S] cluster, facilitating cluster release. On the basis of these findings, we hypothesize that binding of NADP(H) with mitoNEET could be involved in diabetes.

NADP(H) and NAD(H) are both coenzymes of many dehydrogenases involved in metabolic processes. NAD(H) is more important in catabolic reactions in the mitochondrion, while NADP(H) is often used in anabolic reactions such as the biosynthesis of lipids, fatty acids, and steroids, which mainly take place in the cytoplasm. Furthermore, the main domain of mitoNEET is located in the cytoplasm with the N-terminal helix anchoring it to the outer mitochondrial membrane. Thus, it seems reasonable to suggest that the function of mitoNEET may be to sense the level of NADP(H) in the cytoplasm. In the cytosol, redox equilibrium is essential for many biological processes. The increase in the level of free radicals and reactive oxygen species (ROS) leads to oxidative stress, which is considered to be the hallmark of many metabolic and vascular disorders, including both types of diabetes

mellitus. NADH and NADPH are the two major substrates for cytosolic ROS generation by Nox oxidases in vascular smooth muscle (*15*, *16*). In view of this, mitoNEET could play a role as a sensor of oxidative stress in the cell because NADP(H), but not NADH, can bind to mitoNEET.

On the other hand, binding of NADP(H) with mitoNEET destabilizes the [2Fe-2S] cluster, facilitating cluster release. In other words, free iron may accumulate in the mitoNEET sample solution as a result of NADP(H) interaction. Clinical research on links between iron stores and diabetes has suggested that extra iron is stored in body tissues, because the body has no natural way to rid itself of excess iron. High iron levels may either cause damage to muscle tissue, weakening the body's ability to move glucose from the blood into cells and thus interfering with insulin production, or lead to serious problems such as damage to the pancreas, possibly causing diabetes. Several studies have suggested a possible link between high body iron stores and type 2 diabetes (*17*, *18*). Moreover, iron is a strong prooxidant that catalyzes the formation of hydroxyl radicals. Such reactions contribute to tissue damage and increase oxidative stress, thereby potentially altering the risk of type 2 diabetes because the cells that produce insulin are extraordinarily sensitive to damage from oxidation (*19*−*21*). It has previously been shown that mitoNEET is a cellular target of pioglitazone, a member of the thiazolidinedione (TZD) class of insulin-sensitizing drugs used to treat type 2 diabetes (*1*, *22*, *23*). Binding of pioglitazone with mitoNEET enhances the stability of the [2Fe-2S] cluster (*5*). In addition, pioglitazone binds mitoNEET with an affinity significantly higher than that of NADP(H) for mitoNEET. Therefore, pioglitazone may take precedence over NADP(H) in binding with mitoNEET, protecting cells form damaging effects by stabilizing the iron−sulfur clusters in mitoNEET.

However, whether diabetes is related to the destabilizing effect of NADP(H) binding to mitoNEET or whether mitoNEET plays additional roles as an electron carrier, as is the case for ferredoxins, remains puzzling. To clarify the biological association of the binding of NADP(H) with mitoNEET, further biological and biophysical experiments are needed to relate the binding of NADP(H) in vitro to its effect in vivo.

CONCLUSION

This study reports that NADP(H) can bind to human mitoNEET, facilitating release of the [2Fe-2S] clusters from the protein. The adenosine moiety of NADP(H) is involved in the binding to mitoNEET. K55 and H58 are the two major residues of mitoNEET for NADP(H) binding. The proximity of K55 and H58 of one monomer subunit to residues H87′ and R73′, respectively, of the other monomer subunit may be the main structural factor responsible for destabilizing the iron−sulfur clusters by binding of NADP(H). Because H87 and R73 are residues in the [2Fe-2S] cluster coordination loop, the interaction of NADP(H) may disturb the coordination sphere of Fe-1 and the protonation status of H87, thereby interfering with cluster stability.

ACKNOWLEDGMENT

We thank Dr. Xian-Ming Pan (Department of Biological Sciences and Biotechnology, Tsinghua University, Beijing, China) and Dr. Yi Liang (State Key Laboratory of Virology, Wuhan University, Wuhan, China) for helpful comments on the analysis of the ITC data.

SUPPORTING INFORMATION AVAILABLE

NMR titration data to determine the binding of NADP with mitoNEET(44−108) (Figure S1); 2D $^{1}H-^{15}N$ HSQC spectra of mitoNEET(44−108) in the presence of NADPH, NADH, and PO_4^{3-} (Figure S2); ITC measurements for detecting whether NADH can bind to mitoNEET(44−108) (Figure S3); 1D ^{1}H NMR spectra to detect the normal folding of K55Q/H58S mutant and R76Q/K78Q/K89Q mutant mitoNEET(44−108) (Figure S4); ITC measurements for detecting whether NADPH can bind to [K55Q/H58S]mitoNEET(44−108) (Figure S5); 2D $^{1}H-^{15}N$ HSQC spectra of mitoNEET(44−108) for providing the time stability of the [2Fe-2S] cluster (Figure S6); visible−UV absorption measurement of [K55Q/H58S]mitoNEET(44−108) for exploring the influence of the K55Q and H58S mutations (Figure S7); dissociation constants of NADPH with mitoNEET-(44−108) (Table S1); and results of ITC measurements of [R76Q/K78Q/K89Q]mitoNEET(44−108) (Table S2). This material is available free of charge via the Internet at http://pubs.acs.org.

REFERENCES

1. Colca, J. R., McDonald, W. G., Waldon, D. J., Leone, J. W., Lull, J. M., Bannow, C. A., Lund, E. T., and Mathews, W. R. (2004) Identification of a novel mitochondrial protein ("mitoNEET") cross-linked specifically by a thiazolidinedione photoprobe. *Am. J. Physiol. 286*, E252–E260.
2. Nolte, R. T., Wisely, G. B., Westin, S., Cobb, J. E., Lambert, M. H., Kurokawa, R., Rosenfeld, M. G., Willson, T. M., Glass, C. K., and Milburn, M. V. (1998) Ligand binding and co-activator assembly of the peroxisome proliferator-activated receptor-γ. *Nature 395*, 137–143.
3. Wiley, S. E., Paddock, M. L., Abresch, E. C., Gross, L., van der Geer, P., Nechushtai, R., Murphy, A. N., Jennings, P. A., and Dixon, J. E. (2007) The outer mitochondrial membrane protein mitoNEET contains a novel redox-active 2Fe-2S cluster. *J. Biol. Chem. 282*, 23745–23749.
4. Wiley, S. E., Murphy, A. N., Ross, S. A., van der Geer, P., and Dixon, J. E. (2007) MitoNEET is an iron-containing outer mitochondrial membrane protein that regulates oxidative capacity. *Proc. Natl. Acad. Sci. U.S.A. 104*, 5318–5323.
5. Paddock, M. L., Wiley, S. E., Axelrod, H. L., Cohen, A. E., Roy, M., Abresch, E. C., Capraro, D., Murphy, A. N., Nechushtai, R., Dixon, J. E., and Jennings, P. A. (2007) MitoNEET is a uniquely folded 2Fe 2S outer mitochondrial membrane protein stabilized by pioglitazone. *Proc. Natl. Acad. Sci. U.S.A. 104*, 14342–14347.
6. Lin, J., Zhou, T., Ye, K., and Wang, J. (2007) Crystal structure of human mitoNEET reveals distinct groups of iron sulfur proteins. *Proc. Natl. Acad. Sci. U.S.A. 104*, 14640–14645.
7. Hou, X., Liu, R., Ross, S., Smart, E. J., Zhu, H., and Gong, W. (2007) Crystallographic studies of human MitoNEET. *J. Biol. Chem. 282*, 33242–33246.
8. Conlan, A. R., Axelrod, H. L., Cohen, A. E., Abresch, E. C., Nechushtai, R., Paddock, M. L., and Jennings, P. A. (2009) Structural Comparison of a Diabetes Drug Target, Mitoneet, a 2Fe-2S Cluster Protein to Its More Stable Mutant, H87C. *Biophys. J. 96* (Suppl. 1), 67a.
9. Tirrell, T. F., Paddock, M. L., Conlan, A. R., Smoll, E. J., Jr., Nechushtai, R., Jennings, P. A., and Kim, J. E. (2009) Resonance Raman studies of the $(His)(Cys)_3$ 2Fe-2S cluster of MitoNEET: Comparison to the $(Cys)_4$ mutant and implications of the effects of pH on the labile metal center. *Biochemistry 48*, 4747–4752.
10. Zuris, J. A., Paddock, M. L., Abresch, E. C., Conlan, A. R., Nechushtai, R., and Jennings, P. A. (2009) Redox Potential of the Outer-Mitochondrial Membrane 2Fe-2S Protein MitoNEET. *Biophys. J. 96* (Suppl. 1), 240a.
11. Homer, C., Yee, D., Axelrod, H. L., Cohen, A. E., Abresch, E. C., Chang, C., Nechushtai, R., Jennings, P. A., and Paddock, M. L. (2009) Structural Basis for Phosphate Stabilization of the Uniquely Coordinated 2Fe-2S Cluster of the Outer Mitochondrial Membrane Protein MitoNEET. *Biophys. J. 96* (Suppl. 1), 442a–443a.
12. Ho, S. N., Hunt, H. D., Horton, R. M., Pullen, J. K., and Pease, L. R. (1989) Site-directed mutagenesis by overlap extension using the polymerase chain reaction. *Gene 77*, 51–59.
13. Markley, J. L., Bax, A., Arata, Y., Hilbers, C. W., Kaptein, R., Sykes, B. D., Wright, P. E., and Wüthrich, K. (1998) Recommendations for

the Presentation of NMR Structures of Proteins and Nucleic Acids (IUPAC Recommendations 1998). *Pure Appl. Chem. 70*, 117–142.
14. Pitcher, W. H., III, DeRose, E. F., Mueller, G. A., Howell, E. E., and London, R. E. (2003) NMR studies of the interaction of a type II dihydrofolate reductase with pyridine nucleotides reveal unexpected phosphatase and reductase activity. *Biochemistry 42*, 11150-11160.
15. Gupte, S. A., Kaminski, P. M., Floyd, B., Agarwal, R., Ali, N., Ahmad, M., Edwards, J., and Wolin, M. S. (2005) Cytosolic NADPH may regulate differences in basal Nox oxidase-derived superoxide generation in bovine coronary and pulmonary arteries. *Am. J. Physiol. 288*, H13–H21.
16. Lassegue, B., and Clempus, R. E. (2003) Vascular NAD(P)H oxidases: Specific features, expression, and regulation. *Am. J. Physiol. 285*, R277–R297.
17. Hernandez, C., Genesca, J., Ignasi Esteban, J., Garcia, L., and Simo, R. (2000) [Relationship between iron stores and diabetes mellitus in patients infected by hepatitis C virus: A case-control study]. *Med. Clin.* (*Barcelona*) *115*, 21–22.
18. Jiang, R., Manson, J. E., Meigs, J. B., Ma, J., Rifai, N., and Hu, F. B. (2004) Body iron stores in relation to risk of type 2 diabetes in apparently healthy women. *JAMA, J. Am. Med. Assoc. 291*, 711–717.
19. Opara, E. C. (2004) Role of oxidative stress in the etiology of type 2 diabetes and the effect of antioxidant supplementation on glycemic control. *J. Invest. Med. 52*, 19–23.
20. Valko, M., Morris, H., and Cronin, M. T. (2005) Metals, toxicity and oxidative stress. *Curr. Med. Chem. 12*, 1161–1208.
21. Wolff, S. P. (1993) Diabetes mellitus and free radicals. Free radicals, transition metals and oxidative stress in the aetiology of diabetes mellitus and complications. *Br. Med. Bull. 49*, 642–652.
22. Colca, J. R. (2006) Insulin sensitizers may prevent metabolic inflammation. *Biochem. Pharmacol. 72*, 125–131.
23. Yki-Jarvinen, H. (2004) Thiazolidinediones. *N. Engl. J. Med. 351*, 1106–1118.